Nonlinear Analog Spintronics with van der Waals Heterostructures

S. Omar,[1,*] M. Gurram,[1] K. Watanabe,[2] T. Taniguchi,[2] M.H.D. Guimarães,[1] and B.J. van Wees[1]

[1] *The Zernike Institute for Advanced Materials, University of Groningen, Nijenborgh 4, Groningen 9747 AG, Netherlands*

[2] *National Institute for Material Science, 1-1 Namiki, Tsukuba 305-044, Japan*

(Received 26 July 2020; revised 24 October 2020; accepted 16 November 2020; published 17 December 2020)

The existence of nonlinearity in a spintronic device is indispensable for spin-based complex signal-processing operations. Here we measure the presence of electron-spin-dependent nonlinearity in a van der Waals heterostructure spintronic device. We further demonstrate its application for basic analog operations such as essential elements of amplitude modulation and frequency sum (heterodyne detection) on pure spin signals, by exploiting the second-harmonic generation of the spin signal due to nonlinear spin injection. Furthermore, we show that the presence of nonlinearity in the spin signal has an amplifying effect on the energy-dependent conductivity-induced nonlinear spin-to-charge conversion effect. The interaction of the two spin-dependent nonlinear effects in the spin-transport channel leads to a highly efficient modulation of the spin-to-charge conversion effect, which in principle can also be measured without using a ferromagnetic detector. These effects are measured both at room and low temperatures, and are suitable for their applications as nonlinear circuit elements in the fields of advanced spintronics and spin-based neuromorphic computing.

DOI: 10.1103/PhysRevApplied.14.064053

I. INTRODUCTION

Nonlinear elements, such as transistors and diodes that led Shockley and co-workers [1] to lay the foundation for an electronics revolution, underlie modern-day electronics. In a similar way, nonlinear spintronic devices would shape the direction towards spin-based analogs of electronics, specifically to nonvolatile processing-in-memory devices [2–8].

Graphene is one of the most promising materials for spintronics, showing a very long spin lifetime and the longest spin-relaxation length at room temperature [9,10]. Even though some nonlinear effects have been demonstrated in graphene spintronics [11], the magnitudes of such effects were too small for practical applications. There have been recent theoretical studies on other systems such as magnetic insulators [12–14], where nonlinear spin currents can be generated via electric field using optical methods. Additionally, major ideas in the field of graphene spintronics thus far have suggested the possibility of achieving a gate operation employing, for example, a Datta-Das transistor [15,16]. However, a little attention has been paid to achieving nonlinear spintronic operations, such as spin-current amplification and signal processing of spin signals using the junction field effect, similar to the operations in a bipolar-junction field-effect transistor. The presence of nonlinearity in such devices based on all electrical methods is crucial for practical implementation, which has not been explored experimentally and forms a more fundamental building block to replace conventional electronics with spin-based analogs [17–21].

Interestingly, the differential spin-injection efficiency p_{inj} of ferromagnetic (FM) tunnel contacts with atomically flat and pinhole-free thin hexagonal boron nitride (*h*-BN) flakes as a tunnel barrier [22,23] depends on the input dc bias current I [24–26]. This is a nonlinear effect, and renders graphene and *h*-BN heterostructures as a viable platform to demonstrate spin-dependent nonlinear operations.

In this work we perform bias-dependent nonlocal spin-transport measurements in graphene. We distinctively show the smoking gun evidences that *h*-BN tunnel barriers introduce nonlinearity in the spin-injection process, by measuring higher-harmonic spin signals. We further demonstrate the use of such nonlinearity for practical applications, such as amplitude modulation and heterodyne detection operations for future analog graphene spintronics.

The nonlinearity in the spin-injection process produces large spin signals in graphene. As a consequence, we also measure an amplified spin-to-charge conversion effect in the spin-transport channel, which is otherwise unnoticed during spin transport in graphene, due to its small magnitude. This spin-to-charge conversion effect is observed

*s.omar@rug.nl

 © 2020 American Physical Society

due to the energy-dependent band structure of graphene, in the presence of spin accumulation [11,27], and does not require any additional element such as spin-orbit coupling [28,29]. It is purely a nonlinearity-induced effect, which greatly simplifies the need for complex device architectures for measuring the same effect.

Our samples are prepared by the dry van der Waals stacking method [30] using mechanically exfoliated materials to produce graphene encapsulated between *h*-BN flakes. In our devices, the top *h*-BN flake is chosen to be 0.9–1.0 nm thick, or around three layers. This is crucial for obtaining large and nonlinear spin-injection efficiencies. Our electrodes are then patterned using standard electron-beam lithography techniques followed by metal evaporation of Co(65 nm)/Al(3 nm). Some of our electrodes are patterned directly onto graphene, while others are patterned on top of the thin top *h*-BN barrier. We detail the sample fabrication procedure within the Supplemental Material [34].

Our measurements are performed both at liquid-helium temperature and room temperature in vacuum in a flow cryostat. The differential ac signal measurements are performed using the low-frequency (10 Hz) lock-in detection method. For mixed signals (ac+dc) measurements and back-gate application, a Keithley 2410 dc source is used.

II. EXPERIMENTS AND RESULTS

A. Nonlinear spin injection

We start by characterizing the tunnelling behavior of the contacts in our device, Figs. 1(a) and 1(b). Contacts with (without) the *h*-BN tunnel barrier show nonlinear (linear) current-voltage characteristics [inset of Fig. 1(c)] for an applied dc charge current I and the measured voltage drop V_c across the contact in a three-probe measurement geometry. This reflects the tunnel characteristics of the contacts with the *h*-BN tunnel barrier and the Ohmic (transparent) nature of the ones without. Next, we probe the presence of nonlinear behavior in the nonlocal signal v_{nl} in a four-probe measurement geometry. For an input ac current i at frequency $f = 6$ Hz, v_{nl} is measured using the scheme in Fig. 1(a), and its Fourier transform is shown in Fig. 1(c). For a linear device, an applied current at a certain frequency should yield a voltage at the same

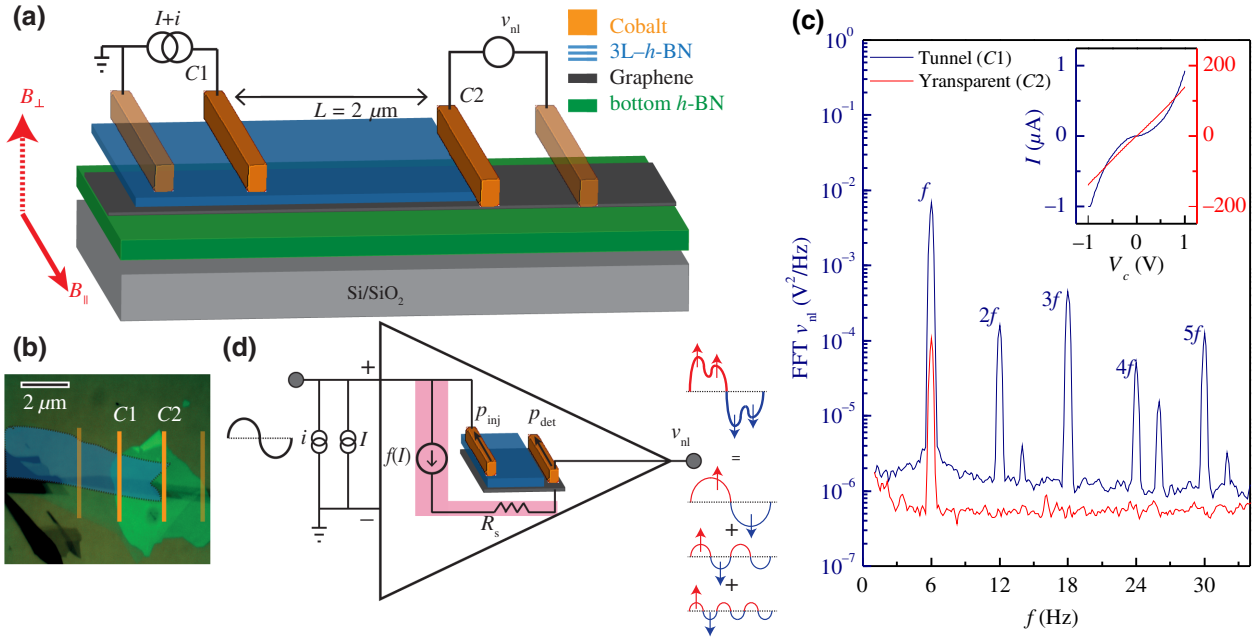

FIG. 1. (a) Graphene encapsulated between a thick *h*-BN at the bottom and a 3L–*h*-BN tunnel barrier on the top. The cobalt (inner) injector electrode $C1$ is located on top of the tunnel barrier and the (inner) detector electrode $C2$ is directly in contact with the graphene flake. The outer injector and detector electrodes (transparent orange) are far enough to be spin sensitive, and serve as reference electrodes. A charge current $i + I$ is applied across $C1$ for spin injection and a nonlocal ac voltage v_{nl} is measured at $C2$ via the lock-in detection method. (b) An optical image of the stack with the actual positions of electrodes drawn schematically. The *h*-BN tunnel barrier is highlighted with false blue color. (c) An ac charge current $i = 50$ nA (20 μA) at $f = 6$ Hz is applied at $C1$ ($C2$) and the Fourier transform of the nonlocal signal measured at $C2$ ($C1$) is plotted in blue (red). In the inset, I-V characteristics of the tunnel contact $C1$ (blue) and the transparent contact $C2$ (red). These measurements are performed at room temperature. (d) The concept of nonlinearity is presented schematically via a circuit diagram. A sinusoidal charge current i along with a dc current I is applied at the input of a nonlinear element (inside the triangle) and a distorted nonsinusoidal spin signal is measured at the output. The harmonic components, which construct the output signal are also shown. The equivalent circuit representing the bias-dependent spin injection [$p_{inj} = f(I)$] and spin transport (R_s) is highlighted in pink.

frequency alone. The appearance of voltage at integral multiples of the input-current frequency, or higher harmonics, is a smoking-gun signature of nonlinearity. We also note additional peaks in our Fourier spectrum of contact $C1$, appearing at 13, 26, and 32 Hz, which likely arise from external interference in our devices, amplified by the nonlinearities of our contacts. In our measurements, higher harmonics at $2f, 3f, \ldots$ appear in $v_{\rm nl}$ only when the tunnel contact $C1$ is used as an injector [blue spectrum in Fig. 1(c)], and are absent when we use the transparent contact $C2$ for injection. This underlines the crucial role of tunnel contacts for introducing nonlinearity in $v_{\rm nl}$.

Thin h-BN tunnel barriers have been known to generate a variable spin-polarization injection [24]. This is a spin-dependent nonlinear effect. Here we explicitly use this property for higher-harmonic spin-current generation in order to perform nonlinear spintronic operations. The concept of our nonlinear spintronic measurements is schematically demonstrated in Fig. 1(d). For an input charge current $i + I$ at a ferromagnetic contact, higher harmonics in the spin signal v_s are measured at the output, due to the nonlinearity in the spin-injection process, present in a spintronic device. To probe the spin-dependent origin of nonlinearity in $v_{\rm nl}$, we perform bias-dependent nonlocal spin-valve (SV) measurements [24]. Here, we apply an ac+dc charge current $i + I$ and measure the first-harmonic response of $v_{\rm nl}$ via the lock-in detection method. An in-plane magnetic field $B_{||}$ is swept to switch the magnetization orientation of $C1$ and $C2$ from parallel to antiparallel and vice versa using the connection scheme in Fig. 1(a). Via SV measurements, we obtain background-free pure spin signal $v_s = (v_{\rm nl}^{\rm p} - v_{\rm nl}^{\rm ap})/2$, where $v_{\rm nl}^{\rm ap}(v_{\rm nl}^{\rm p})$ is the nonlocal signal $v_{\rm nl}$ measured at the (anti)parallel magnetization-direction alignment of the electrodes $C1$ and $C2$, as labeled in Fig. 2(a). In order to obtain the bias dependence of the spin signal, we measure $v_{\rm nl}^{p({\rm ap})}$ as a function of I, as shown in Fig. 2(d), and obtain v_s. At $I = 0$, there is a very small spin signal $v_s \sim 3$ nV [black dash line in Fig. 2(d)]. Note that here a transparent contact $C2$ (with no h-BN tunnel barrier) is used to measure the spin signal. Transparent contacts are able to detect spin signals in graphene, albeit with a smaller polarization [31]. We also ensure via additional measurements that the transparent contact $C2$ is indeed spin sensitive. For this, we perform SV measurements using $C2$ as the injector and $C1$ as the detector [32,33], and again measure the spin-valve effect (see Supplemental Material [34]).

Now, on applying I across the injector electrode, in line with the previous studies on Gr–h-BN tunnel-barrier systems [24,25], v_s increases in magnitude and changes its sign on reversing the polarity of I [Fig. 2(d)]. We note that there is a spin-independent component in our nonlocal signal, in the order of 100 μV in the first harmonic. This spin-independent background, which is removed by performing the difference between parallel and antiparallel alignment of our electrodes, has a probable charge [35] or thermal origin [36,37].

Next, in order to investigate if the higher-harmonic peaks in $v_{\rm nl}$ in Fig. 1(c) also have spin-dependent origin, we selectively measure higher harmonics in $v_{\rm nl}$, using the lock-in-detection method. We unambiguously measure the spin-valve effect in second, third, and fourth (see Supplemental Material [34]) harmonic $v_{\rm nl}$ via SV measurements and its bias dependence, as shown in Figs. 2(b), 2(c), 2(e), and 2(f). The measured higher-harmonic spin signals clearly suggest the presence of nonlinear processes in the spin signal.

To confirm the spin-dependent origin of the nonlinearity in the spin signal, we perform Hanle spin-precession measurements on first-, second-, and third-harmonic spin signals. Here, for a fixed in-plane magnetization configuration of the injector-detector electrodes (parallel or antiparallel), as labeled in Figs. 2(a)–2(c), a magnetic field $B_\perp$ is applied perpendicular to the plane of the device, as shown in Fig. 1(a). The injected in-plane spins diffuse towards the detector and precess around $B_\perp$ with the Larmor frequency $\omega_L \propto B_\perp$. The whole dynamics is given by the Bloch equation, $D_s\nabla^2\vec{\mu_s} - \vec{\mu_s}/\tau_s + \vec{\omega_L} \times \vec{\mu_s} = 0$, with the spin-diffusion constant D_s, spin-relaxation time τ_s, spin accumulation $\vec{\mu_s} = v_s/p_{\rm det}$ in the transport channel, and the spin-diffusion length $\lambda_s = \sqrt{D_s\tau_s}$. The measured first-, second-, and third-harmonic Hanle curves are fitted with the solution to the Bloch equation. From the fitting, we consistently obtain $D_s \sim 0.02$ m^2 s^{-1} and $\tau_s \sim$ 650–700 ps resulting in $\lambda_s \sim 4$ μm for the first and higher-harmonic measurements in Figs. 2(g)–2(i). Since the spin-transport parameters are the same for all harmonics, we conclude that the higher-harmonic spin signals do not have its origin in the spin-transport process, and pinpoint the origin of the spin-dependent nonlinearity in the spin signal to the spin-injection process itself.

To understand the concept of nonlinearity during spin injection, we now develop an analytical framework. As the differential spin-injection polarization depends on the input dc bias current I, the expression for $p_{\rm inj}$ using the Tailor expansion around $I = 0$ with a small ac charge current i can be written as

$$p_{\rm inj}(i)|_{I=0} = p_0(1 + C_1 i + C_2 i^2 + \cdots), \tag{1}$$

where $p_{\rm inj} = p_0$ in the absence of nonlinear processes, which are enabled via the nonzero constants $C_1, C_2, \ldots$. Now, using the relation $v_s = p_{\rm inj}R_s p_{\rm det} i$, where R_s is the effective spin resistance of graphene [38] and $p_{\rm det}$ is the spin-detection efficiency of the detector electrode, we obtain

$$v_s \propto p_0 i + p_0 C_1 i^2 + \cdots, \tag{2}$$

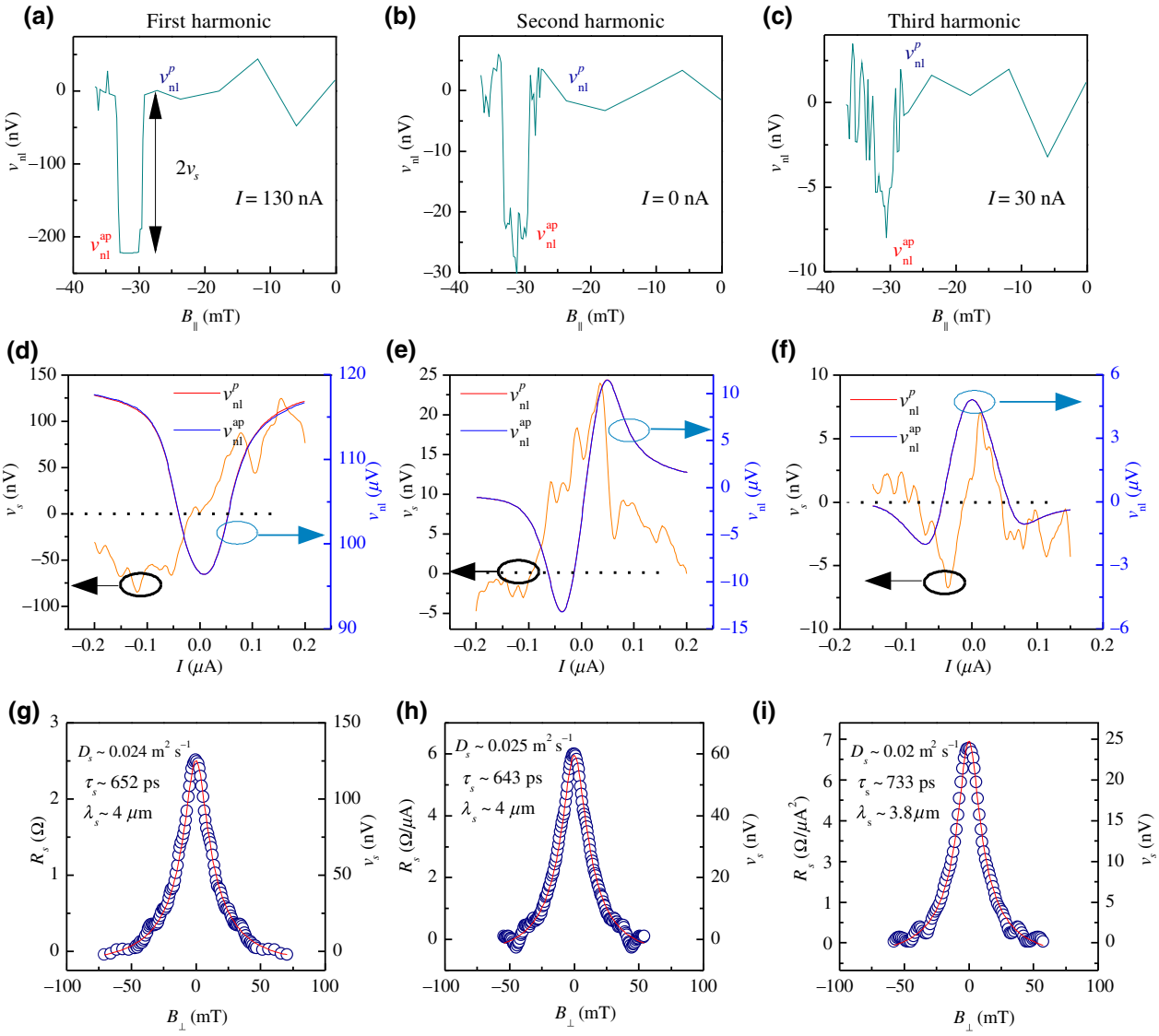

FIG. 2. (a) First-, (b) second-, and (c) third-harmonic spin-valve measurements. Here, a constant background offset (approximately 100 μV for first, and approximately μV for second and third harmonic) is subtracted from the signal, for a clear representation. (d) First-, (e) second-, and (f) third-harmonic spin signal v_s (in orange) is plotted at the left y axis, and nonlocal signal v_{nl} is plotted at the right y axis, as a function of I applied at $C1$, using the measurement geometry in Fig. 1(a). The ac injection current i is kept fixed at 50 nA. v_{nl}^{p} (red) and v_{nl}^{ap} (blue) are the nonlocal signal v_{nl} measured at the parallel and antiparallel magnetization configurations of the injector-detector electrodes, respectively. (g) First-, (h) second-, and (i) third-harmonic Hanle spin signal v_s as a function of out-of-plane magnetic field $B_{\perp}$. Hanle data is symmetrized in order to remove the linear background and is offset to zero. SV measurements in (a)–(f) are performed at room temperature, and Hanle curves in (g)–(h) are measured at 4 K.

which enables us to measure the presence of higher-harmonic spin signals $\propto i^2, i^3, \ldots$ due to the nonlinearity introduced by the spin-injection process in Eq. (1).

As shown in the spin-transport measurements in Fig. 2, the nonlinearity can be experimentally probed by using the mixed signal (ac+dc) measurements. When an input current $i + I$ is applied to such a nonlinear system, the expression for the first-harmonic spin signal v_s, obtained by replacing i with $i + I$ in Eq. (2), acquires a different function form (see Supplemental Material [34] for derivation) and contains a bias I dependent term:

$$v_s \sim [p_0(1 + 2C_1 I)]\, R_s p_{\mathrm{det}} i. \tag{3}$$

As a consequence of the nonlinearity present in the spin signal, Eq. (2), additional terms with the mixing of i and I appear, and now $p_{\mathrm{inj}} \sim p_0(1 + 2C_1 I)$ is obtained instead of p_0 (at $I = 0$). For such case, one would expect a gain in $p_{\mathrm{inj}} \propto I$. Indeed, corroborating with the hypothesis in

Eq. (3), v_s increases in magnitude with the applied dc bias I and reverses its sign with the dc current polarity [Fig. 2(d)].

Similarly, the expressions for nth ($n \geq 2$) harmonic components of $v_s \propto (C_{n-1} + C_n I) i^n$ due to nonzero C_js are obtained using the mixed signal analysis (see Supplemental Material [34] for detailed expressions). Here, the contribution from C_{n-1}, i.e., the nth-order term in Eq. (2) would appear even if only the ac current is applied. In the presence of a nonzero I, the higher-order term C_n would also contribute to the nth-order spin signal and introduce the dc bias dependence on the spin signal.

For SV measurements in our device, we can only measure the even harmonic spin-signal, i.e., second [Figs. 2(b) and 2(e)] and fourth (Supplemental Material [34]) harmonic using the pure ac current injection ($I = 0$). However, similar to the first-harmonic spin signal, higher odd (third) harmonic spin signal [Figs. 2(c) and 2(f)] can be measured unambiguously only with the application of the dc bias. When a nonzero I is applied, the contribution of even harmonic signals couples to the odd harmonic spin signals, and now the odd harmonic responses can also be measured. The dominance of only even harmonic components in the spin signal is peculiar, and is not clear at the moment. Also, the bias-dependent behavior of higher-harmonic spin signals can be explained via the expressions obtained from the mixed-signal analysis only near the zero bias, where higher ($\geq$ fifth) harmonic components do not play a major role. A complete understanding of this behavior warrants the inclusion of higher-order terms in the expression for contact polarization as well as higher-harmonic SV measurements for the estimation of the proportionality constant C_j ($\geq$ fifth harmonic).

B. Analog signal processing of spin signal due to nonlinear effects

The presence of nonlinearity, which gives rise to signal amplification, is fundamental to analog signal-processing operations [39]. In our spintronic device, we exploit the spin-dependent nolinearity and demonstrate its applications straightaway by performing the spin analogs of well established analog electronic operations.

1. Amplitude modulation

For amplitude-modulation signal processing, a modulating input i_m at signal frequency f_m is applied to a nonlinear element, along with a reference input $i_{\rm ref}$ at frequency $f_{\rm ref}$ [40]. For the conventional definition of AM, $f_m < f_{\rm ref}$, and $i_{\rm ref}$ are modulated with the frequency f_m, and the amplitude of the carrier signal $i_{\rm ref}$ is modulated with the magnitude of the input signal i_m.

Note that the basic functionality of AM can be demonstrated with any value pair of (f_m,$f_{\rm ref}$). Here, for sake of simplicity we choose $f_{\rm ref} = f_m$, and exploit the second-harmonic generation of spin signal due to nonlinear spin injection, for basic demonstration of the AM experiment. We demonstrate the modulation in the carrier magnitude that is proportional to the input signal i_m [41]. For this, the reference signal $i_{\rm ref}$ is applied along i_m in our nonlinear spintronic device [Fig. 3(a)]. As a result of nonlinear spin injection, second-harmonic generation, along with higher-harmonic generation also occurs, and the output spin signal $v_s \propto (i_{\rm ref} + i_m)^2$ is detected at frequency $2f$. For a constant $i_{\rm ref}$, if $i_m << i_{\rm ref}$, the measured spin signal is $\propto i_{\rm ref}^2 + 2 i_{\rm ref} i_m$, implying that the effect is linear in i_m, with a spin-signal offset proportional to $i_{\rm ref}^2$ at the detection frequency $2f$ (second-harmonic response).

In order to measure this effect, we inject $i_{\rm ref} = 200$ nA and modulate i_m in the range of 0–120 nA (both at $f = 7$ Hz) at the injector [Fig. 1(a)]. We measure the second harmonic v_s via SV measurements. The measured spin signal is linear in i_m [Fig. 3(b)] and thus the device is modulating the output in the desired way. For the other situation, i.e., when $i_m >> i_{\rm ref}$, $v_s \propto (i_m)^2$. In this case, we fix $i_{\rm ref} = 30$ nA and modulate i_m in the range 30–60 nA. The measured response of v_s [Fig. 3(c)] clearly deviates from the earlier measured linear response in Fig. 3(c). However, due to the contribution of higher-order terms to the second-harmonic signal, the measurement in Fig. 3(c) is better explained by the fourth-order polynomial fit instead of a parabolic fit.

2. Heterodyne detection

As another demonstration of signal processing, in a heterodyne detection method the input signal frequencies are not equal, i.e., $f_m \neq f_{\rm ref}$, and one obtains the signal at the heterodyne frequencies $f_{\rm ref} \pm f_m$ at the output of the nonlinear element [40,42]. In order to realize this operation, $i_{\rm ref}$ at the frequency $f_{\rm ref} = 2f$ and i_m at $f_m = f$ are applied at the injector input [Fig. 3(d)]. The nonlinear component of the spin signal v_s is $\propto [i_{\rm ref} \sin(2\pi f t) + i_m \sin(2\pi 2 f t)]^2$. If i_m =0, one would expect the spin signal v_s at $2f$ due to second-harmonic generation. Interestingly, for $i_m \neq 0$, $v_s \propto i_{\rm ref} i_m$ can also be detected at the first- ($f = 2f - f$) and third- ($3f = 2f + f$) harmonic components. In this way, using heterodyne detection, we also demonstrate an analog spin-signal multiplier at frequencies f and $3f$.

In our measurements, for $i_m = 0$ and $i_{\rm ref} = 200$ nA ($f = 7$ Hz), only the second-harmonic spin signal is measured [Fig. 3(e)]. When we also apply $i_m = 150$ nA at the input frequency $2f$, spin-valve signals of similar magnitudes are detected at frequencies both at f and $3f$ [Fig. 3(f)], which is a clear demonstration of *heterodyne* detection of spin signals. Note that earlier there is no measurable odd (first and third) harmonic spin signal at $I = 0$ [Figs. 2(d) and 2(f)] due to low injection polarization and high noise present in the signal. Now, using the heterodyne detection method we can clearly measure v_s in the first harmonic even without applying I. In fact, this effect is equivalent

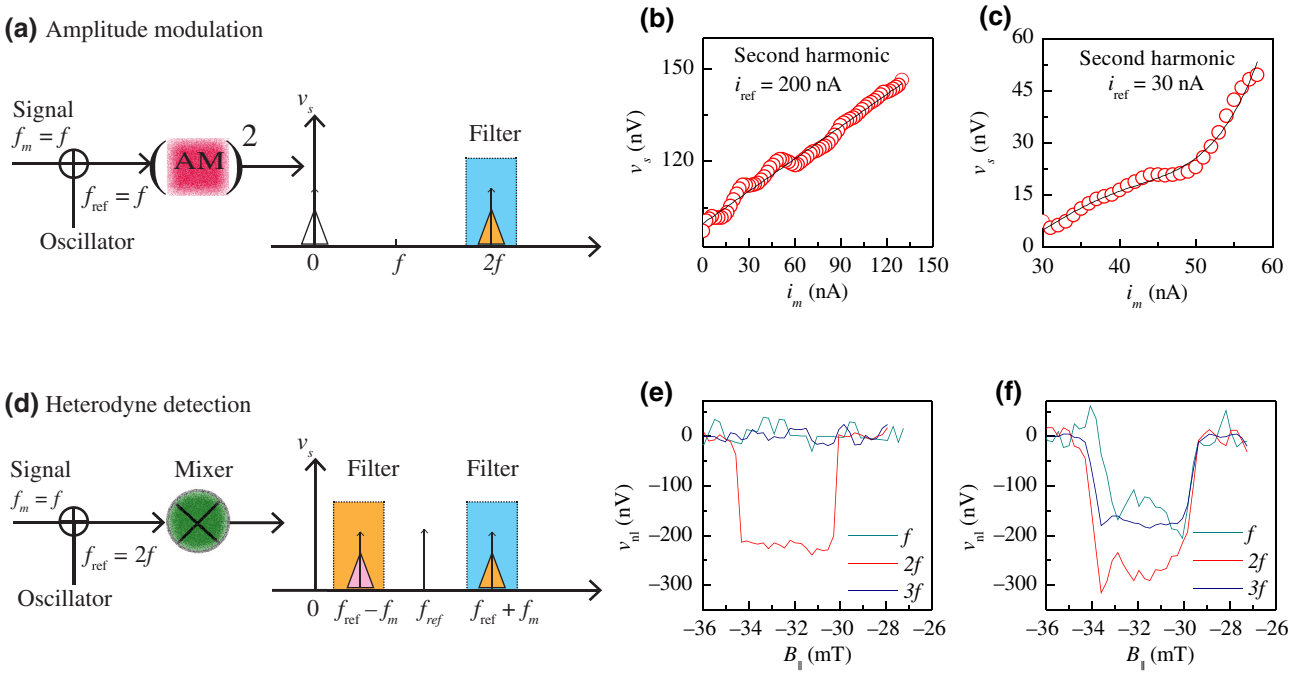

FIG. 3. A sum signal of the message signal with frequency f_m and the carrier signal with frequency f_{ref} is prepared outside the device and fed at the input terminal. (a) Amplitude modulation (AM) scheme. (b) AM measurement of the spin signal v_s for $i_m << i_{ref}$ and the linear fit (black) (c) $i_m \geq i_{ref}$ and the nonlinear fit (fourth-order polynomial). (d) Heterodyne detection scheme (e) for $i_m = 0$ no spin signal is present at the frequency f and $3f$. The spin-valve signal at $2f$ is present because of second-harmonic generation due to nonlinear spin injection. (f) For $i_m \neq 0$, due to the frequency shifting of the signal present at $2f$ to f and $3f$, equal strength signal appears at both frequencies. Both measurements are performed at room temperature. SV measurements in (e),(f) are offset to zero for clear representation.

to applying a *dc* current, as both heterodyne and ac+dc measurements couple the higher-harmonic spin signals to the first-harmonic spin signal. This method can be used to detect spin signals at low frequencies where the spin-dependent noise dominates in spintronic circuits [43,44]. Furthermore, the method can also be used as an electrical analog of the heterodyne detection in the field on optical spin-noise spectroscopy [45,46].

C. Nonlinear spin-to-charge conversion

So far we demonstrate that the nonlinearity present in the spin signal in a Gr–*h*-BN heterostructure has its origin in the spin-injection process, not in the spin-transport parameters. However, the nonlinearity in the spin injection has an important consequence, and can amplify another nonlinear effect present in a small magnitude, i.e., spin-to-charge conversion [11,27] in the spin-transport channel. The effect requires the energy-dependent conductivity of the transport channel and the presence of spin accumulation as prerequisites. A nonlocal charge signal v_c due to energy-dependent spin-to-charge conversion is given by

$$v_c = C_0 \mu_s^2 = C_0 (p_{\mathrm{inj}} R_s e)^2 i^2, \tag{4}$$

where C_0 is a proportionality constant (see Supplemental Material [34] for details), and we use the relation $\mu_s = v_s e / p_{\mathrm{det}}$ to obtain the v_c-i dependence.

In the earlier study of the energy-dependent spin-to-charge conversion [11], nonmagnetic electrodes are used to measure the effect because spin polarization of the detector is not relevant for measuring the charge signal. In principle, the same effect can be measured even via ferromagnetic electrodes as they can also measure the charge voltage. In our measurements of the spin-to-charge conversion effect, we perform conventional spin-transport measurements, and separate the spin-to-charge conversion effect from the spin signal judiciously, via a careful data analysis. If a single FM injector-detector pair is used, we can obtain v_c in Eq. (4) from the spin-transport data, by taking the average of parallel and antiparallel spin signals $R_{\mathrm{nl}}^{\mathrm{p(ap)}}$. The reason being the spin-to-charge conversion-induced signal is only sensitive to the magnitude of the spin signal, but not to its sign Eq. (4). During the magnetization reversal of either of the injector-detector electrodes, spin-to-charge conversion v_c does not change its sign while the spin signal does. This is valid for both first- and higher- (second-, third-,. . .) harmonic signals. In this way, by averaging $R_{\mathrm{nl}}^{\mathrm{p}}$ and $R_{\mathrm{nl}}^{\mathrm{ap}}$, we obtain only the signal due to spin-to-charge conversion effect,

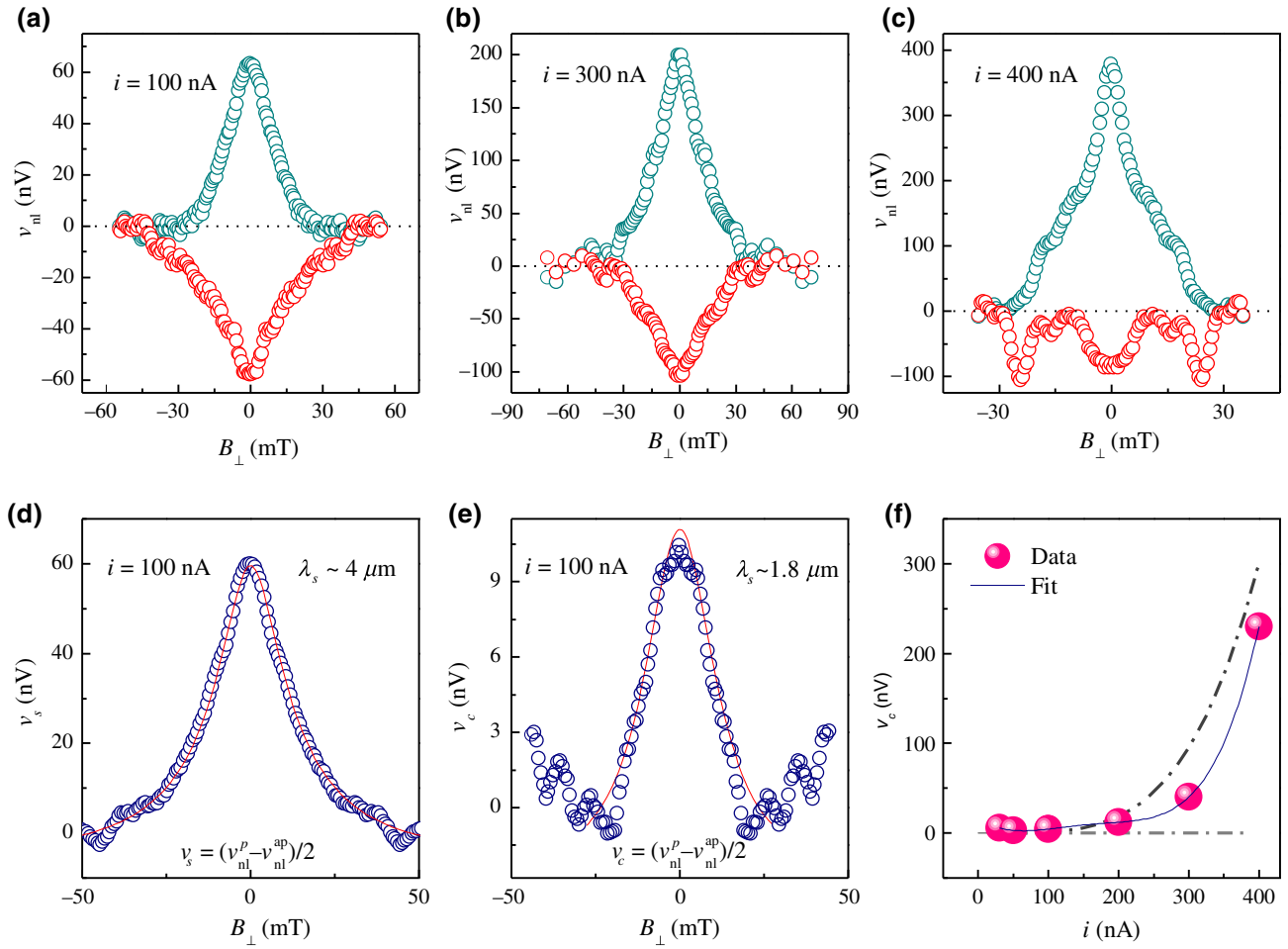

FIG. 4. Second-harmonic Hanle measurements in the parallel (green) and antiparallel (red) configuration for i_{ac}= (a) 100 nA, (b) 300 nA, and (c) 400 nA. The enhancement in the spin-accumulation-induced charge signal v_c with i is visible in the asymmetry between $v_{\rm nl}^{\rm p}$ and $v_{\rm nl}^{\rm ap}$ with respect to the spin-independent background (dashed black line). The measured data is symmetrized in order to remove the spin-independent linear component present in the data and is offset to zero. All measurements are performed at 4 K. Second-harmonic Hanle spin-precession measurements of (d) the spin signal v_s and (e) the spin-accumulation-induced charge signal v_c. Both data are obtained from (a) for $i = 100$ nA and fitted with the solution to the Bloch equation. From the fit in (d), (e), we obtain $\lambda_s \sim 4$ μm and 1.8 μm for the spin and charge signal, respectively. (f) $v_c - i$ dependence for the second-harmonic data is fitted (blue curve) with a fourth-order polynomial function. The dark (light) gray dashed line is the calculated magnitude of second-harmonic component of v_c due to the nonlinear (linear) spin injection.

while the difference of these two signals gives us pure spin signal devoid of the contribution from spin-to-charge conversion.

Now, to probe the spin-to-charge conversion effect and the spin-dependent origin of the nonlocal charge voltage, we perform Hanle measurements. Since the spin-to-charge conversion is a second-harmonic effect Eq. (4) for the applied charge current i, we inject a pure ac current i in the range 100–400 nA and measure the second-harmonic response of $v_{\rm nl}^{\rm p(ap)}$ as a function of $B_\perp$ using the measurement geometry in Fig. 1(a). In our measurements, we observe an asymmetry between the magnitudes of $v_{\rm nl}^{\rm p}$ and $v_{\rm nl}^{\rm ap}$ in Figs. 4(a)–4(c), which is present in a small magnitude for $i = 100$ nA, and grows rapidly for $i = 400$ nA to such an extent that the Hanle dephasing of $v_{\rm nl}$ is measured properly only in the parallel configuration.

To understand the origin of this asymmetry, we plot the nonlocal charge voltage $v_c = (v_{\rm nl}^{\rm p} + v_{\rm nl}^{\rm ap})/2$ [Fig. 4(e)] and the spin signal $v_s = (v_{\rm nl}^{\rm p} - v_{\rm nl}^{\rm ap})/2$ [Fig. 4(d)]. The Hanle-like shape of $v_c(B_\perp)$ in Fig. 4(e) immediately confirms that indeed the nonlocally measured charge voltage v_c has the spin-dependent origin, and is reduced to zero in the absence of spin accumulation (at $B_\perp \sim 40$ mT). Next, due to its square dependence on μ_s in Eq. (4), v_c should decay with the characteristic spin-relaxation length $\lambda_s/2$ instead of λ_s [27]. In order to verify this hypothesis Eq. (4), we fit v_c-$B_\perp$ dependence in Fig. 4(e) with the solution to the Bloch equation, and obtain $\lambda_s \sim 2$ μm, which

is about half the spin-relaxation length obtained via the Hanle spin-precession measurements on the spin signal v_s [Fig. 4(d)]. The same effect appears in the first harmonic v_c due to its coupling with the second-harmonic effect in the presence of a nonzero I (see Supplemental Material [34]). Note that in the earlier study [11], it was not possible to perform Hanle measurements, and extract spin-transport parameters, due to the small magnitude of the measured charge signal. Owing to the large spin-injection efficiency via *h*-BN tunnel barriers, and improved spin-transport parameters in fully encapsulated graphene, we could create large spin-accumulation magnitudes. In this way, we unambiguously establish the spin-dependent origin and the square dependence of the nonlocal charge voltage on spin accumulation via Hanle measurements.

Lastly, the v_c-i dependence is plotted in Fig. 4(f). The dark (light) gray dashed line is the calculated magnitude of v_c while considering the contribution from nonlinear (linear) spin injection with $i^4(i^2)$ dependence on the injected current (see Supplemental Material [34] for details). The measured data is in a close agreement with the calculated v_c due to the nonlinear spin injection, and is better fitted with a fourth-order polynomial than a parabolic function. Clearly, such efficient modulation of spin-to-charge conversion cannot be explained only via the linear spin-injection process, and the contribution from the nonlinear processes has to be taken into account. In conclusion, Gr–*h*-BN heterostructures due to the presence of nonlinear spin injection offer a highly efficient platform to probe nonlinear spin-to-charge conversion effect. The interaction of the two nonlinear effects produces a measurable effect without needing any additional effect such as spin-orbit coupling [28,29].

III. CONCLUSIONS

To summarize, we demonstrate the presence of spin-dependent nonlinearity in a spintronic device via all electrical measurements, and use this to generate higher harmonics in the spin signal. This effect is the key ingredient in signal processing, and opens the door for the development of the field of analog spintronics, following the pathway of the electronics revolution. Our results suggest that nonlinearity can be exploited in multiple ways to manipulate spin information such as via complex signal processing and spin-to-charge conversion, and develop advanced multifunctional spintronic devices [10,11,18,27,47] and spin-based neuromorphic computing [5].

ACKNOWLEDGMENTS

We acknowledge J. G. Holstein, H.H. de Vries, T. Schouten, H. Adema, and A. Joshua for their technical assistance. We thank B.N. Madhushankar for the help in sample preparation, and A. Kamra for critically reading the manuscript. Growth of hexagonal boron nitride crystals is supported by the Elemental Strategy Initiative conducted by the MEXT, Japan and the CREST(JPMJCR15F3), JST. MHDG acknowledges financial support from the Dutch Research Council (NWO VENI 15093). This research work is funded by the the Graphene flagship core 1 and core 2 program (Grants No. 696656 and No. 785219), Spinoza Prize (for B.J.v.W.) by the Netherlands Organization for Scientific Research (NWO) and supported by the Zernike Institute for Advanced Materials.

[1] W. Shockley, M. Sparks, and G. K. Teal, *p-n* Junction transistors, Phys. Rev. **83**, 151 (1951).
[2] B. Divinskiy, S. Urazhdin, S. O. Demokritov, and V. E. Demidov, Controlled nonlinear magnetic damping in spin-hall nano-devices, Nat. Commun. **10**, 5211 (2019).
[3] V. E. Demidov, S. Urazhdin, A. Anane, V. Cros, and S. O. Demokritov, Spin–orbit-torque magnonics, J. Appl. Phys. **127**, 170901 (2020).
[4] X. Cheng, J. A. Katine, G. E. Rowlands, and I. N. Krivorotov, Nonlinear ferromagnetic resonance induced by spin torque in nanoscale magnetic tunnel junctions, Appl. Phys. Lett. **103**, 082402 (2013).
[5] J. Torrejon, M. Riou, F. A. Araujo, S. Tsunegi, G. Khalsa, D. Querlioz, P. Bortolotti, V. Cros, K. Yakushiji, A. Fukushima, H. Kubota, S. Yuasa, M. D. Stiles, and J. Grollier, Neuromorphic computing with nanoscale spintronic oscillators, Nature **547**, 428 (2017).
[6] M. R. Pufall, W. H. Rippard, S. Kaka, T. J. Silva, and S. E. Russek, Frequency modulation of spin-transfer oscillators, Appl. Phys. Lett. **86**, 082506 (2005).
[7] N. Locatelli, V. Cros, and J. Grollier, Spin-torque building blocks, Nat. Mater. **13**, 11 (2014).
[8] M. Tarequzzaman, T. Böhnert, M. Decker, J. D. Costa, J. Borme, B. Lacoste, E. Paz, A. S. Jenkins, S. Serrano-Guisan, C. H. Back, R. Ferreira, and P. P. Freitas, Spin torque nano-oscillator driven by combined spin injection from tunneling and spin hall current, Commun. Phys. **2**, 1 (2019).
[9] A. Avsar, H. Ochoa, F. Guinea, B. Özyilmaz, B. J. van Wees, and I. J. Vera-Marun, Colloquium: Spintronics in graphene and other two-dimensional materials, Rev. Mod. Phys. **92**, 021003 (2020).
[10] M. Gurram, S. Omar, and B. J. van Wees, Electrical spin injection, transport, and detection in graphene-hexagonal boron nitride van der Waals heterostructures: Progress and perspectives, 2D Mater. **5**, 032004 (2018).
[11] I. J. Vera-Marun, V. Ranjan, and B. J. van Wees, Nonlinear detection of spin currents in graphene with non-magnetic electrodes, Nat. Phys. **8**, 313 (2012).
[12] T. N. Ikeda and M. Sato, High-harmonic generation by electric polarization, spin current, and magnetization, Phys. Rev. B **100**, 214424 (2019).
[13] H. Ishizuka and M. Sato, Theory for shift current of bosons: Photogalvanic spin current in ferrimagnetic and antiferromagnetic insulators, Phys. Rev. B **100**, 224411 (2019).
[14] T. N. Ikeda, Generation of DC, AC, and second-harmonic spin currents by electromagnetic fields in an

inversion-asymmetric antiferromagnet, Condens. Matter. **4**, 92 (2019).
[15] S. Datta and B. Das, Electronic analog of the electro-optic modulator, Appl. Phys. Lett. **56**, 665 (1990).
[16] M. Gmitra and J. Fabian, Proximity Effects in Bilayer Graphene on Monolayer WSe_2: Field-Effect Spin Valley Locking, Spin-Orbit Valve, and Spin Transistor, Phys. Rev. Lett. **119**, 146401 (2017).
[17] M. Zeng, L. Shen, M. Zhou, C. Zhang, and Y. Feng, Graphene-based bipolar spin diode and spin transistor: Rectification and amplification of spin-polarized current, Phys. Rev. B **83**, 115427 (2011).
[18] Y. Acremann, X. W. Yu, A. A. Tulapurkar, A. Scherz, V. Chembrolu, J. A. Katine, M. J. Carey, H. C. Siegmann, and J. Stöhr, An amplifier concept for spintronics, Appl. Phys. Lett. **93**, 102513 (2008).
[19] Y. Wang, Y. Liu, and B. Wang, Graphene spin diode: Strain-modulated spin rectification, Appl. Phys. Lett. **105**, 052409 (2014).
[20] M. E. Flatté, Z. G. Yu, E. Johnston-Halperin, and D. D. Awschalom, Theory of semiconductor magnetic bipolar transistors, Appl. Phys. Lett. **82**, 4740 (2003).
[21] J. Fabian and I. Žutic, Spin-polarized current amplification and spin injection in magnetic bipolar transistors, Phys. Rev. B **69**, 115314 (2004).
[22] M. Gurram, S. Omar, S. Zihlmann, P. Makk, C. Schönenberger, and B. J. van Wees, Spin transport in fully hexagonal boron nitride encapsulated graphene, Phys. Rev. B **93**, 115441 (2016).
[23] G.-H. Lee, Y.-J. Yu, C. Lee, C. Dean, K. L. Shepard, P. Kim, and J. Hone, Electron tunneling through atomically flat and ultrathin hexagonal boron nitride, Appl. Phys. Lett. **99**, 243114 (2011).
[24] M. Gurram, S. Omar, and B. J. v. Wees, Bias induced up to 100% spin-injection and detection polarizations in ferromagnet/bilayer-hBN/graphene/hBN heterostructures, Nat. Commun. **8**, 248 (2017).
[25] J. C. Leutenantsmeyer, J. Ingla-Aynés, M. Gurram, and B. J. van Wees, Efficient spin injection into graphene through trilayer hBN tunnel barriers, J. Appl. Phys. **124**, 194301 (2018).
[26] T. Zhu, S. Singh, J. Katoch, H. Wen, K. Belashchenko, I. Žutic, and R. K. Kawakami, Probing tunneling spin injection into graphene via bias dependence, Phys. Rev. B **98**, 054412 (2018).
[27] I. J. Vera-Marun, V. Ranjan, and B. J. van Wees, Nonlinear interaction of spin and charge currents in graphene, Phys. Rev. B **84**, 241408(R) (2011).
[28] T. S. Ghiasi, A. A. Kaverzin, P. J. Blah, and B. J. van Wees, Charge-to-spin conversion by the Rashba-edelstein effect in two-dimensional van der Waals heterostructures up to room temperature, Nano Lett. **19**, 5959 (2019).
[29] C. K. Safeer, J. Ingla-Aynés, F. Herling, J. H. Garcia, M. Vila, N. Ontoso, M. R. Calvo, S. Roche, L. E. Hueso, and F. Casanova, Room-temperature spin Hall effect in Graphene/MoS2 van der Waals heterostructures, Nano Lett. **19**, 1074 (2019).
[30] P. J. Zomer, M. H. D. Guimarães, J. C. Brant, N. Tombros, and B. J. van Wees, Fast pick up technique for high quality heterostructures of bilayer graphene and hexagonal boron nitride, Appl. Phys. Lett. **105**, 013101 (2014).
[31] W. Han, K. Pi, W. Bao, K. M. McCreary, Y. Li, W. H. Wang, C. N. Lau, and R. K. Kawakami, Electrical detection of spin precession in single layer graphene spin valves with transparent contacts, Appl. Phys. Lett. **94**, 222109 (2009).
[32] A. Spiesser, Y. Fujita, H. Saito, S. Yamada, K. Hamaya, S. Yuasa, and R. Jansen, Hanle spin precession in a two-terminal lateral spin valve, Appl. Phys. Lett. **114**, 242401 (2019).
[33] R. Jansen, A. Spiesser, H. Saito, Y. Fujita, S. Yamada, K. Hamaya, and S. Yuasa, Nonlinear Electrical Spin Conversion in a Biased Ferromagnetic Tunnel Contact, Phys. Rev. Appl. **10**, 064050 (2018).
[34] See Supplemental Material at http://link.aps.org/supplemental/10.1103/PhysRevApplied.14.064053 for a detailed description of the nonlinear spin-injection model, mixed-signal analysis, derivation for nonlinear spin-to-charge conversion (first and second harmonic), additional measurements on spin-to-charge conversion, spin injection via the transparent contact, and fourth-harmonic spin signal.
[35] F. Volmer, M. Drögeler, E. Maynicke, N. von den Driesch, M. L. Boschen, G. Güntherodt, C. Stampfer, and B. Beschoten, Suppression of contact-induced spin dephasing in graphene/MgO/Co spin-valve devices by successive oxygen treatments, Phys. Rev. B **90**, 165403 (2014).
[36] S. Kasai, S. Hirayama, Y. K. Takahashi, S. Mitani, K. Hono, H. Adachi, J. Ieda, and S. Maekawa, Thermal engineering of non-local resistance in lateral spin valves, Appl. Phys. Lett. **104**, 162410 (2014).
[37] J. Renard, M. Studer, and J. A. Folk, Origins of Nonlocality Near the Neutrality Point in Graphene, Phys. Rev. Lett. **112**, 116601 (2014).
[38] $R_s = R_{\mathrm{sq}}\lambda_s \exp(-\frac{L}{\lambda_s})/2w$ is the effective spin-resistance with channel sheet resistance R_{sq} and spin relaxation length λ_s. L and w are the length (injector-detector separation) and width of the transport channel is the spin detection efficiency of the detector electrode.
[39] B. Razavi, *Fundamentals of Mircroelectronics* (Wiley, New York, 2013), 2nd ed.
[40] S. H. Nawab, Alan V. Oppenheim and Alan S. Willsky, *Signals and Systems* (Pearson, 1996), 2nd ed.
[41] In order to demonstrate the full AM functionality, the precondition $f_{\mathrm{ref}} >> f_m$ must be satisfied in order to satisfy the Nyquist criterion, i.e., $f_{\mathrm{ref}} \geq 2f_m$. Otherwise, the demodulation of the signal cannot be performed accurately.
[42] A. S. Sedra and K. C. Smith, *Microelectronic Circuits* (Oxford University Press, New York, 2009), 6th ed.
[43] S. Omar, M. H. D. Guimarães, A. Kaverzin, B. J. van Wees, and I. J. Vera-Marun, Spin relaxation 1/f noise in graphene, Phys. Rev. B **95**, 081403(R) (2017).
[44] S. Omar, B. J. van Wees, and I. J. Vera-Marun, Two-channel model for spin-relaxation noise, Phys. Rev. B **96**, 235439 (2017).
[45] S. Cronenberger and D. Scalbert, Quantum limited heterodyne detection of spin noise, Rev. Sci. Instrum. **87**, 093111 (2016).
[46] P. Sterin, J. Wiegand, J. Hübner, and M. Oestreich, Optical Amplification of Spin Noise Spectroscopy via Homodyne Detection, Phys. Rev. Appl. **9**, 034003 (2018).
[47] B. Behin-Aein, D. Datta, S. Salahuddin, and S. Datta, Proposal for an all-spin logic device with built-in memory, Nat. Nanotechnol. **5**, 266 (2010).